AIP | Journal of Applied Physics

Toward the creation of terahertz graphene injection laser

V. Ryzhii, M. Ryzhii, V. Mitin, and T. Otsuji

Citation: J. Appl. Phys. **110**, 094503 (2011); doi: 10.1063/1.3657853
View online: http://dx.doi.org/10.1063/1.3657853
View Table of Contents: http://jap.aip.org/resource/1/JAPIAU/v110/i9
Published by the American Institute of Physics.

Toward the creation of terahertz graphene injection laser

V. Ryzhii,[1,a)] M. Ryzhii,[1] V. Mitin,[2] and T. Otsuji[3]
[1]*Computational Nanoelectronics Laboratory, University of Aizu, Aizu-Wakamatsu 965-8580, Japan*
[2]*Department of Electrical Engineering, University at Buffalo, Buffalo, New York 14260-1920, USA*
[3]*Research Institute for Electrical Communication, Tohoku University, Sendai 980-8577, Japan*

(Received 9 September 2011; accepted 27 September 2011; published online 3 November 2011)

We study the effect of population inversion associated with the electron and hole injection in graphene p-i-n structures at the room and slightly lower temperatures. It is assumed that the recombination and energy relaxation of electrons and holes are associated primarily with the interband and intraband processes assisted by optical phonons. The dependences of the electron-hole and optical phonon effective temperatures on the applied voltage, the current-voltage characteristics, and the frequency-dependent dynamic conductivity are calculated. In particular, we demonstrate that at low and moderate voltages, the injection can lead to a pronounced cooling of the electron-hole plasma in the device i-section to the temperatures below the lattice temperature. However at higher voltages, the voltage dependences can be ambiguous exhibiting the S-shape. It is shown that the frequency-dependent dynamic conductivity can be negative in the terahertz (THz) range of frequencies at certain values of the applied voltage. The electron-hole plasma cooling substantially reinforces the effect of negative dynamic conductivity and promotes the realization of terahertz lasing. On the other hand, the heating of optical phonon system can also be crucial affecting the realization of negative dynamic conductivity and terahertz lasing at the room temperatures. © *2011 American Institute of Physics*. [doi:10.1063/1.3657853]

I. INTRODUCTION

The gapless energy spectrum of electrons and holes in graphene layers (GLs), graphene bilayers (GBLs), and non-Bernal stacked multiple graphene layers (MGLs)[1–3] opens up prospects of creating terahertz (THz) lasers based on these graphene structures. In such structures, GLs and MGLs with optical[4–10] and injection[11] pumping can exhibit the interband population inversion and negative dynamic conductivity in the THz range of frequencies and, hence, can serve as active media in THz lasers. The most direct way to create the interband population in GLs and MGLs is to use optical pumping[4] with the photon energy $\hbar\Omega_0$ corresponding to middle- and near-infrared (IR) ranges. In this case, the electrons and holes, photogenerated with the kinetic energy $\hbar\Omega_0/2$, transfer their energy to optical phonons and concentrate in the states near the Dirac point.[4,12,13] The amplification of THz radiation from optically pumped GL structures observed recently[14,15] is attributed to the interband stimulated emission. However, the optical pumping with relatively high photon energies exhibits drawbacks. First of all, the optical pumping, which requires complex setups, might be inconvenient method in different applications of the prospective graphene THz lasers. Second, the excessive energy being received by the photogenerated electro-hole plasma from pumping source can lead to its marked heating because of the redistribution of the initial electron and hole energy $\hbar\Omega_0/2$ among all carries due to rather effective inter-carrier collisions. The latter results in a decrease of the ratio of the quasi-Fermi energies μ_e and μ_h to the electron-hole effective temperature T that, in turn, complicate achieving of sufficiently large values of the dynamic conductivity. As demonstrated recently,[16,17] the negative conductivity at the THz frequencies is very sensitive to the ratio of the photon energy $\hbar\Omega$ and the optical phonon energy $\hbar\omega_0$, as well as to the relative efficiency of the inter-carrier scattering and the carrier scattering on optical phonons. The decay of nonequilibrium optical phonons also plays an important role.

The abovementioned complications can be eliminated in the case of pumping resulting in the generation in GLs electrons and holes with relatively low initial energies. This in part can be realized in the case of optical pumping with $\hbar\Omega_0/2 < \hbar\omega_0$.[16] Taking into account that in GLs $\hbar\omega_0 \simeq 0.2$eV, in the case of CO_2 laser as a pumping source, $\Omega_0/\omega_0 \simeq 0.5$. As shown,[16] in such a case, the electron-hole plasma can even be cooled, so that $T < T_0$, where T_0 is the lattice (thermostat) temperature. Another weakly heating or even cooling pumping method which can provide low effective temperature T (including $T < T_0$) is the injection pumping of electrons from n-section and holes from p-section in GL and MGL structures with p-i-n junctions.

In this paper, we study the injection phenomena in GL and MGL p-i-n structures and calculate their characteristics important for THz lasers. The idea to use p-n junctions in GLs was put forward and briefly discussed by us previously.[11] Here, we consider more optimal designs of the structures (with a sufficiently long i-section) and account for realistic mechanisms of recombination at elevated temperatures (at the room temperature and slightly below).

The paper is organized as follows. In Sec. II, we describe the device structures under consideration and principles of their operation. The pertinent equations of the model governing the balance of electrons, holes, and optical

[a)]Author to whom correspondence should be addressed. Electronic mail: v-ryzhii@u-aizu.ac.jp.

phonons (rate equations) are presented in Sec. III. These equations are reduced to an equation governing the electron-hole effective temperature. The solution of this equation in Secs. IV and V (both analytically in limiting cases and numerically) allows us to find the effective temperature of optical phonons and the current as functions of the applied voltage, the structural parameters, and the lattice temperature. In Sec. VI, the obtained characteristics of the injected electron-hole plasma are used to calculate the dependence of the dynamic conductivity of the latter as a function of the signal THz frequency and other quantities. Section VII deals with the model limitations and discussion. In Sec. VIII, we draw the main conclusions.

II. DEVICE MODEL

We consider devices which comprise a GL or a MGL structure with several non-Bernal stacked GLs. It is assumed that the sections of GLs adjacent to the side contacts are doped (p- and n-sections). The device structure under consideration is shown in Fig. 1(a). The dc voltage V is applied between the side contacts to provide the forward bias of the p-i-n junction. Due to doping of the side sections with the acceptor and donor sheet concentration Σ_i, the electron and hole Fermi energies counted from the Dirac point are $\mu_e = \mu_i$ and $\mu_h = -\mu_i$, where $\mu_i \simeq \hbar v_F \sqrt{\pi \Sigma_i}$, $\hbar$ is the reduced Planck constant and $v_F \simeq 10^8$ cm/s is the characteristic velocity of the carrier spectrum in GLs. Instead of doping of the side sections, the p- and n-sections can be created using highly conducting gates over these sections to which the gate voltages $V_p = -V_g < 0$ and $V_n = V_g > 0$ are applied.[11] In this case, the chemically doped p- and n-sections are replaced by the electrically induced sections (see, for instance,[18,19]) as shown in Fig. 2(b). In single-GL structures, $\mu_i \propto \sqrt{V_g/W_g}$, where W_g is the spacing between the GL and the gate. In the case of MGL structures, the situation becomes more complex due to the screening of the transverse electric field in GLs

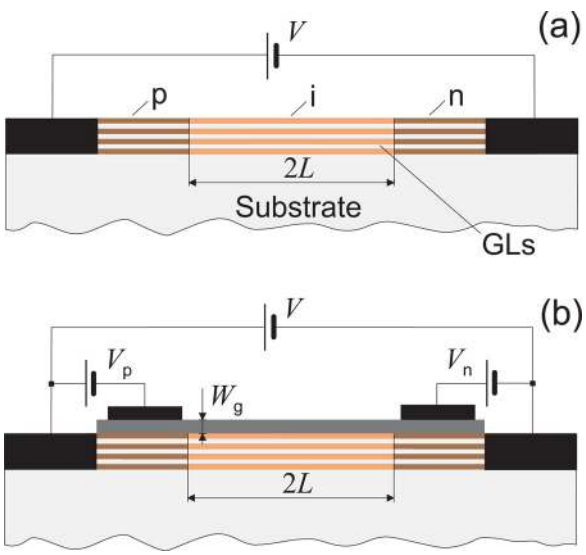

FIG. 1. (Color online) Schematic view of the cross-sections of MGL laser structures (a) with chemically doped n- and p-sections and (b) with such section electrically induced by the side gate-voltages $V_p = -V_g$ and $V_n = V_g > 0$.

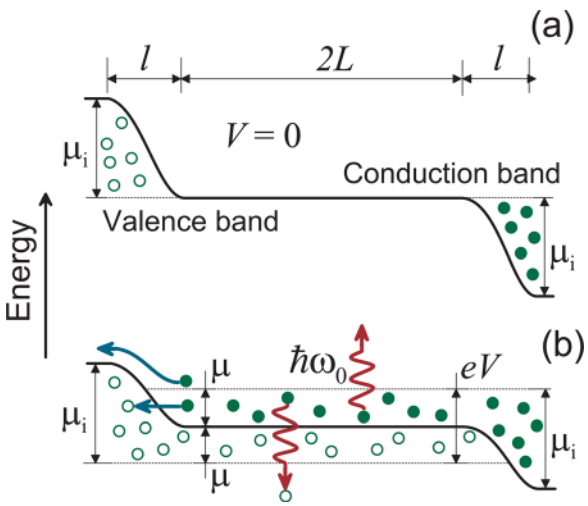

FIG. 2. (Color online) Band profiles of a GL in p-i-n junctions (a) at $V = 0$ and (b) at forward bias $V > 0$. Opaque and open circles correspond to electrons and holes, respectively. Wavy arrows show some interband (recombination) and intraband transitions assisted by optical phonons. Smooth arrows indicate tunneling and thermionic leakage processes.

(Ref. 19) although the effective electric doping can be achieved in MGL structures with about dozen GLs. For definiteness, in the following, we shall consider primarily the devices with chemically doped p-i-n junctions. As shown below, under certain conditions, the frequency-dependent dynamic conductivity of the GL or MGL structures can be negative in a certain range of the signal frequencies. In this case, the self-excitation of THz modes propagating in the substrate serving as a dielectric waveguide (in the direction perpendicular to the injection current) and lasing is possible. The metal gates in the devices with electrically induced p-i and i-n junctions can also serve as the slot-line waveguides for THz waves. Apart from this, the self-excitation of surface plasmons (plasmon-polaritons) is possible as well (see, for instance, Refs. 4, 6, and 8–10).

When the p-i-n junction under consideration is forward biased by the applied voltage V, the electrons and holes are injected to the i-section from the pertinent doped side sections. The injected electrons and holes reaching the opposite doped section can recombine at it due to the interband tunneling or escape the i-section due to the thermionic processes. The band profiles in the structures under consideration at $V = 0$ and at the forward bias $V > 0$ are shown in Fig. 2. Since the probability of such tunneling is a very sharp function of angle of incidence, the leakage flux due to the tunneling electrons (holes) is much smaller that the flux of injected electrons (holes). The currents associated with the tunneling and thermionic leakage of electrons at the p-i-junction and holes at the i-n-junction depend on the electric field at the pertinent barriers and the applied voltage V. Because the relative role of the leakage currents diminishes with increasing length of the i-section $2L$, width of the p-i- and i-n-junctions l, and the barrier height at these junctions μ_i, we shall neglect it. The pertinent conditions will be discussed in the following. Thus, it is assumed that the main fractions of the injected electrons and holes recombine inside the i-section. The recombination of electrons and holes in GLs at not too

low temperatures is mainly determined by the emission of optical photons.[20] Considering the sub-threshold characteristics (i.e., the states below the threshold of lasing) and focusing on the relatively high-temperature operation, we shall account for this recombination mechanism and disregard others[21–24] including the mechanism[25] associated with the tunneling between the electron-hole puddles (if any).[26–29] Due to high net electron and hole densities in MGL structures with sufficient number of GLs, the latter mechanism can be effectively suppressed.[25] We also assume that the net recombination rate in the whole i-section is much smaller than the fluxes of injected electrons and holes.

III. EQUATIONS OF THE MODEL

Due to rather effective inter-carrier scattering, the electron and hole distribution functions (at least at not too high energies) can be very close to the Fermi distribution functions with quasi-Fermi energies μ_e and μ_h and the electron-hole effective temperature T. The latter quantities are generally different from those in equilibrium (without pumping) at which $\mu_e = \mu_h = 0$ and $T = T_0$. At the pumping of an intrinsic GL structure, $\mu_e = -\mu_h = \mu$, where generally $\mu > 0$. Under these conditions, the quasi-Fermi energy μ in the i-section (neglecting the leakage and recombination in the lowest approximation), is given by [see Fig. 2(b)]

$$\mu = eV/2, \tag{1}$$

where e is the electron charge.

The terminal current between the side contacts (per unit length in the lateral direction perpendicular to the current), which coincides with the recombination current, is given by

$$J = 2eLR_0^{inter} \tag{2}$$

The rate of the optical phonon-assisted interband transitions (recombination rate) R_0^{inter} and the rate of the intraband energy relaxation associated with optical phonons R_0^{intra} can be calculated using the following simplified formulas[9,16] (see, also Ref. 20):

$$R_0^{inter} = \frac{\Sigma_0}{\tau_0^{inter}}\left[(\mathcal{N}_0+1)\exp\left(\frac{2\mu-\hbar\omega_0}{T}\right)-\mathcal{N}_0\right] = \frac{\Sigma_0}{\tau_0^{inter}}\left[(\mathcal{N}_0+1)\exp\left(\frac{eV-\hbar\omega_0}{T}\right)-\mathcal{N}_0\right], \tag{3}$$

$$R_0^{intra} = \frac{\Sigma_0}{\tau_0^{intra}}\left[\left[(\mathcal{N}_0+1)\exp\left(-\frac{\hbar\omega_0}{T}\right)-\mathcal{N}_0\right]. \tag{4}$$

Here, τ_0^{inter} and τ_0^{intra} are the pertinent characteristic times (relatively slow dependent on μ and T), Σ_0 is the equilibrium electron and hole density, and $\mathcal{N}_0$ is the number of optical phonons. Here and in all equations in the following, T and T_0 are in the energy units. When the optical phonon system is close to equilibrium, one can put $\mathcal{N}_0 = [\exp(\hbar\omega_0/T_0)-1]^{-1} = \mathcal{N}_0^{eq}$. For numerical estimates, we set $\bar{R}_0^{inter} = \Sigma_0/\tau_0^{inter} \simeq 10^{23}\,\mathrm{cm^{-2}s^{-1}}$.[20] Equations (2) and (3) yield the following general formula for the structure current-voltage characteristic:

$$J = \frac{2eL\Sigma_0}{\tau_0^{inter}}\left[(\mathcal{N}_0+1)\exp\left(\frac{eV-\hbar\omega_0}{T}\right)-\mathcal{N}_0\right]. \tag{5}$$

Naturally, at $V = 0$, $T = T_0$, so that $\mathcal{N}_0 = [\exp(\hbar\omega_0/T_0)-1]^{-1}$ and $J = 0$. At $V > 0$, due to contributions of the recombination and injection to the energy balance of the electron-hole plasma in the i-section, the electron-hole effective temperature T can deviate from the lattice temperature T_0. The number of optical phonons $\mathcal{N}_0$ can also be different from its equilibrium value $\mathcal{N}_0^{eq}$. Since $\hbar\omega_0$ is large, in a wide range of temperatures (including the room temperatures), $\hbar\omega_0 \gg T_0$.

The electron-hole plasma gives up the energy $\hbar\omega_0$ in each act of the optical phonon emission (interband and intraband) and receives the same energy absorbing an optical phonon. Hence, the net rate of the energy transfer from and to the electron hole-plasma due to the interaction with optical phonons is equal to $2L\hbar\omega_0\left(R_0^{inter}+R_0^{intra}\right)$. Considering Eqs. (3) and (4) and taking into account that the Joule power associated with the injection current is equal to $Q = JV = 2eLR_0^{inter}V$, an equation governing the energy balance in the electron-hole plasma in the i-section can be presented as

$$\frac{eV}{\tau_0^{inter}}\left[(\mathcal{N}_0+1)\exp\left(\frac{eV-\hbar\omega_0}{T}\right)-\mathcal{N}_0\right] = \frac{\hbar\omega_0}{\tau_0^{inter}}\left[(\mathcal{N}_0+1)\exp\left(\frac{eV-\hbar\omega_0}{T}\right)-\mathcal{N}_0\right] + \frac{\hbar\omega_0}{\tau_0^{intra}}\left[(\mathcal{N}_0+1)\exp\left(-\frac{\hbar\omega_0}{T}\right)-\mathcal{N}_0\right]. \tag{6}$$

Here, the left-hand side corresponds to the power received by the electron-hole plasma in the i-section from the pumping source, whereas the right-hand side corresponds to the power transferred to or received from the optical phonon system.

The number of optical phonons is governed by an equation which describes the balance between their generation in the interband and intraband transitions and decay due to the anharmonic contributions to the interatomic potential, leading to the phonon-phonon scattering and in the decay of optical phonons into acoustic phonons. This equation can be presented in the form

$$\frac{(\mathcal{N}_0-\mathcal{N}_0^{eq})}{\tau_0^{decay}} = \frac{1}{\tau_0^{inter}}\left[(\mathcal{N}_0+1)\exp\left(\frac{eV-\hbar\omega_0}{T}\right)-\mathcal{N}_0\right] + \frac{1}{\tau_0^{intra}}\left[(\mathcal{N}_0+1)\exp\left(-\frac{\hbar\omega_0}{T}\right)-\mathcal{N}_0\right], \tag{7}$$

where τ_0^{decay} is the optical phonon decay time. This time can be markedly longer than τ_0^{inter} and τ_0^{intra}, particularly in suspended GLs, so that parameter $\eta_0^{decay} = \tau_0^{decay}/\tau_0^{inter}$ can exceed or substantially exceed unity. As shown,[30–34] τ_0^{decay} in GLs is in the range of 1–10 ps. As calculated recently,[17] the characteristic times τ_0^{inter} and τ_0^{intra} can be longer than 1 ps. If so, the situation when $\eta_0^{decay} < 1$ appears also to be feasible. The optical phonon decay time might be fairly short depending on the type of the substrate.

Instead of Eq. (7), one can use the following equation which explicitly reflexes the fact that the energy received by

the electron-hole plasma from the external voltage source goes eventually to the optical phonon system

$$\eta_0^{decay}\frac{eV}{\hbar\omega_0}\left[(\mathcal{N}_0+1)\exp\left(\frac{eV-\hbar\omega_0}{T}\right)-\mathcal{N}_0\right]=\mathcal{N}_0-\mathcal{N}_0^{eq}. \tag{8}$$

Using Eqs. (6) and (7) or Eqs. (6) and (8), one can find T and $\mathcal{N}_0$ as functions of V and then calculate the current-voltage characteristic invoking Eq. (5), as well as the dynamic characteristics.

Equation (8) yields

$$\mathcal{N}_0=\frac{\mathcal{N}_0^{eq}+\eta_0^{decay}\frac{eV}{\hbar\omega_0}\exp\left(\frac{eV-\hbar\omega_0}{T}\right)}{1+\eta_0^{decay}\frac{eV}{\hbar\omega_0}\left[1-\exp\left(\frac{eV-\hbar\omega_0}{T}\right)\right]}. \tag{9}$$

Substituting $\mathcal{N}_0$ given by Eqs. (9) to (6), we arrive at the following equation for T:

$$\begin{aligned}&\frac{1+\eta_0^{decay}\frac{eV}{\hbar\omega_0}\left[1-\exp\left(\frac{eV-\hbar\omega_0}{T}\right)\right]}{\mathcal{N}_0^{eq}+\eta_0^{decay}\frac{eV}{\hbar\omega_0}\exp\left(\frac{eV-\hbar\omega_0}{T}\right)}\\&\times\left[\eta_0\frac{(\hbar\omega_0-eV)}{\hbar\omega_0}\exp\left(\frac{eV}{T}\right)+1\right]\\&+\eta_0\frac{(\hbar\omega_0-eV)}{\hbar\omega_0}\left[\exp\left(\frac{eV-\hbar\omega_0}{T}\right)-1\right]\exp\left(\frac{\hbar\omega_0}{T}\right)\\&-\exp\left(\frac{\hbar\omega_0}{T}\right)+1=0.\end{aligned} \tag{10}$$

The ratio $\eta_0=\tau_0^{intra}/\tau_0^{inter}$ is actually a function of μ and T. The $\eta_0-\mu$ and η_0-T dependences are associated with the linearity of the density of states in GLs as a function of energy. To a good approximation, these dependences can be described[16] by function $\eta_0=\hbar^2\omega_0^2/(6\mu^2+\pi^2T^2)$ with $\eta_0\propto(\hbar\omega_0/T)^2$ at $\mu\ll T$ and $\eta_0\propto(\hbar\omega_0/\mu)^2$ at $\hbar\omega_0>\mu\gg T$. Thus, considering Eq. (1), η_0 in Eq. (10) is given by

$$\eta_0=\frac{2\hbar^2\omega_0^2}{(3e^2V^2+2\pi^2T^2)}. \tag{11}$$

Introducing the effective temperature of the optical phonon system Θ such that $\mathcal{N}_0=[\exp(\hbar\omega_0/\Theta)-1]^{-1}$, i.e.,

$$\Theta=\frac{\hbar\omega_0}{\ln(1+\mathcal{N}_0^{-1})}, \tag{12}$$

and substituting $\mathcal{N}_0$ from Eq. (9) to Eq. (11), one can relate Θ and T. Then, calculating the T–V dependences using Eq. (10), one can find the pertinent Θ–V dependences.

IV. EFFECTIVE TEMPERATURES AND CURRENT-VOLTAGE CHARACTERISTICS (ANALYTICAL ANALYSIS)

A. Low voltages

In particular, at $V=0$, Eqs. (8) and (10) naturally yield $\mathcal{N}_0=\mathcal{N}_0^{eq}$ and $T=T_0$. At sufficiently low voltages when $(\eta_0^{decay}eV/\hbar\omega_0)\ll 1$, the solutions of Eqs. (9) and (10) can be found analytically. In this case, $\mathcal{N}_0\simeq\mathcal{N}_0^{eq}$. Considering this, at low voltages, Eq. (10) yields

$$T\simeq T_0\left[1-\frac{eV}{\hbar\omega_0}\frac{\eta_0^{eq}}{(1+\eta_0^{eq})}\right]<T_0, \tag{13}$$

where η_0^{eq} is the value of η_0 at $V\ll\hbar\omega_0/e$, i.e., $\eta_0^{eq}\simeq 5$.[16] As follows from Eq. (13), an increase in the applied voltage V leads to a decrease in the effective temperature of the electron-hole plasma (its cooling).

Using Eqs. (5) and (13) at low voltages, we also obtain

$$\frac{J}{J_0}\simeq\frac{eV}{T_0}\frac{\eta_0^{eq}}{(1+\eta_0^{eq})}\exp\left(-\frac{\hbar\omega_0}{T_0}\right). \tag{14}$$

Here, the current J is normalized by its characteristic value $J_0=2eL\Sigma_0/\tau_0^{inter}=2eL\bar{R}^{inter}$.

B. Special cases

In the special case $V=\hbar\omega_0/e$ (i.e., $V\simeq 0.2$V), from Eqs. (9), (10), and (12), we obtain

$$T=\frac{\hbar\omega_0}{\ln\left(\frac{1+\eta_0^{decay}+\mathcal{N}_0^{eq}}{\eta_0^{decay}+\mathcal{N}_0^{eq}}\right)}, \tag{15}$$

$$\mathcal{N}_0=\mathcal{N}_0^{eq}+\eta_0^{decay}. \tag{16}$$

One can see that in this case

$$\mathcal{N}_0=\frac{1}{\exp(\hbar\omega_0/T)-1}, \tag{17}$$

i.e., $\Theta=T$ and

$$J=J_0. \tag{18}$$

At $T_0=300$ K and $2L=20\,\mu$m, one obtains $J_0\simeq 32$ A/cm. As follows from Eqs. (15)–(17) at $V=\hbar\omega_0/e$, T and Θ tend to T_0 if η_0^{decay} tends to zero and $T=\Theta$, and they both increase proportionally to η_0^{decay} as η_0^{decay} tends to infinity. Thus, at $V=\hbar\omega_0/e$ and $\eta_0^{decay}\sim 1$, the effective temperatures are fairly high: $T=\Theta\sim\hbar\omega_0/\ln 2$ ($T=\Theta\sim 3300$ K). It is worth noting that J at $V=\hbar\omega_0/e$ is independent of parameter η_0^{decay}.

In interesting (but nonrealistic) limiting case $\eta_0^{decay}=0$, from Eq. (8), we immediately obtain $\mathcal{N}_0=\mathcal{N}_0^{eq}$. In such a case, $T=T_0$ both at $V=0$ and $V=\hbar\omega_0/e$. If $V=\hbar\omega_0/2e$, one obtains

$$T\simeq\frac{T_0}{2[1-(T_0/\hbar\omega_0)\ln(2+\eta_0)]}, \tag{19}$$

$$J\simeq J_0(\eta_0+1)\exp\left(-\frac{\hbar\omega_0}{T_0}\right)\ll J_0. \tag{20}$$

At $T_0=300$ K, Eqs. (19) and (20) yield $T\simeq 0.60\ T_0=180$ K and $J\simeq 31$ mA/cm at $T_0=300$ K and $T\simeq 0.569\ T_0=114$ K and 0.64 mA/cm at $T_0=200$ K.

C. Long optical phonon decay time

In the case of relatively long optical decay time, when $\eta_0^{decay} \gg 1$ at $V \lesssim \hbar\omega_0/e$, neglecting terms of the order of $\mathcal{N}_0^{eq}/\eta_0^{decay} \simeq \exp(-\hbar\omega_0/T_0)/\eta_0^{decay}$, from Eq. (10), we obtain

$$T \simeq \frac{eV}{\ln\left\{\dfrac{1+\eta_0^{decay}(eV/\hbar\omega_0)}{\eta_0^{decay}(eV/\hbar\omega_0)+\eta_0[(eV/\hbar\omega_0)-1]}\right\}}. \quad (21)$$

At $V = \hbar\omega_0/e$, Eq. (21) yields the same value of T as Eq. (15) provided $\eta_0^{decay} \gg \mathcal{N}_0^{eq}$.

V. EFFECTIVE TEMPERATURES AND CURRENT-VOLTAGE CHARACTERISTICS (NUMERICAL RESULTS)

To obtain T–V and Θ–V dependences in wide ranges of parameter η_0^{decay} and the applied voltage V, Eqs. (9)–(12) were solved numerically. Figures 3 and 4 show the voltage dependences of effective temperatures T and Θ calculated for different values η_0^{decay} and $T_0 = 300$ and 200 K. One can see from Fig. 3 that the electron-hole effective temperature markedly decreases with increasing voltage, so that $T < T_0$ in a certain voltage range [see also Eq. (13)] and then starts to rise. In the range of relatively high voltages ($V \lesssim \hbar\omega_0/e$), the T–V dependence is steeply rising [in line with analytical formula given by Eq. (21)] with $T > T_0$ or even $T \gg T_0$. However, it is intriguing that in a rather narrow voltage range where V is about some value V_d, the T–V dependences are ambiguous, so that these dependences as a whole are of the S-shape. The appearance of the S-shape characteristics can be attributed to a decrease in parameter η_0 with increasing T [see Eq. (11)]. This corresponds to a decrease in τ_0^{intra} and, hence, to an essential intensification of the intraband transitions, particularly, those associated with the reabsorption of nonequilibrium optical phonons when T increases. This is because at high electron-hole effective temperatures, the intraband transitions assisted by optical phonons take place between relatively high energy states with their elevated density. When V exceeds some "disruption" voltage V_d, the net power acquired by the electron-hole plasma can be compensated by the intraband energy relaxation on optical phonons only at sufficiently high T. As a result, in this case, the electron-hole temperature jumps to the values corresponding to higher branch of the T–V dependence. Thus, the "observable" T–V dependences and their consequences can as usual exhibit hysteresis instead of the S-behavior. One needs to point out that if the above temperature-dependent parameter η_0 is replaced in calculations by a constant, the calculated T–V dependences become unambiguous, although they exhibit a steep increase in the range $V \sim V_d$.

The behavior of T as a function of V markedly depends on parameters η_0^{decay} and η_0. The width of the voltage range where $T < T_0$ increases when parameter η_0^{decay} becomes smaller with increasing voltage. Simultaneously, the depth of the T–V sag dependent with $T < T_0$ increases with decreasing η_0^{decay} as well as with decreasing T_0. At small η_0^{delay}, the electron-hole cooling can be rather strong, particularly when $T_0 = 200$ K. This is natural because faster decay of optical phonons prevents their accumulation (heating) and promotes the electron-hole plasma cooling when the Joule power is smaller than the power transferred from electrons and holes to optical phonons. It worth noting that the voltage range where the T–V dependence is ambiguous widens with increasing η_0^{decay}.

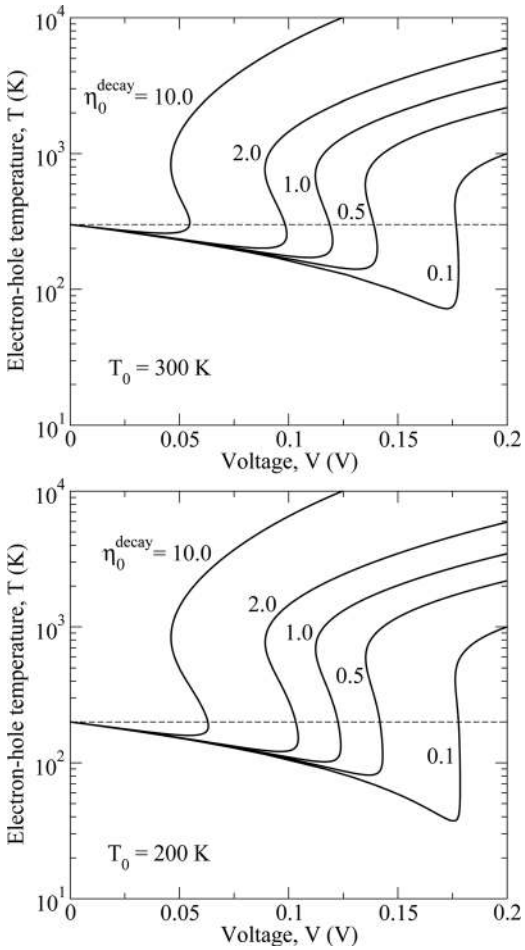

FIG. 3. Electron-hole effective temperature T as function of applied voltage V for different values of η_0^{decay} and T_0. Dashed lines correspond to $T = 300$ K (upper panel) and $T = 200$ K (lower panel).

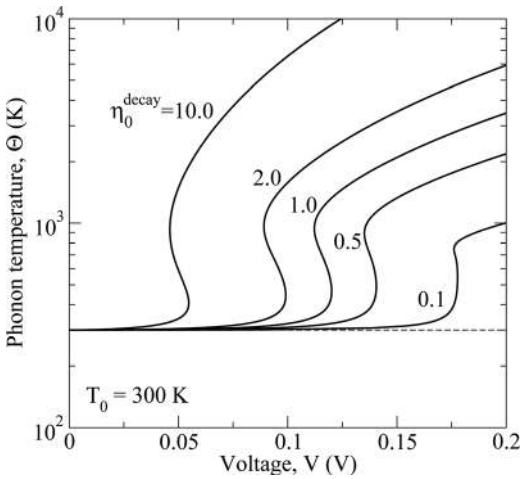

FIG. 4. Optical phonon effective temperature Θ as function of applied voltage V for different values of η_0^{decay}. Dashed line corresponds to $\Theta = 300$ K.

As seen from Fig. 4, the optical phonon effective temperature also exhibits a *S*-shape voltage dependence. However, contrary to the electron-hole effective temperature, $\Theta \geq T_0$ at all the voltages is under consideration. The values of Θ at relatively high voltages steeply increase with increasing parameter η_0^{decay}.

Comparing the *T*–*V* dependences calculated for different lattice temperatures, one can find that at moderate and large values of η_0^{delay}, these dependences are virtually independent of T_0. This is because in such a case, the number of optical phonons $\mathcal{N}_0 \gg \mathcal{N}_0^{eq}$ and, hence, $\Theta \gg T_0$ even at not too high voltages, so that the role of equilibrium optical phonons is weak.

Invoking Eq. (5), the *T*–*V* dependences obtained above can be used to find the current-voltage characteristics. Figure 5 shows the *J*–*V* characteristics calculated using Eq. (5) and the *T*–*V* and Θ–*V* dependences obtained numerically. As a consequence of the S-shape *T*–*V* and Θ–*V* dependences, the *J*–*V* characteristics (as well as the voltage dependences of the dynamic conductivity considered in the following) are also of the *S*-shape. According to Figs. 3 and 5, the *T*–*V* and *J*–*V* characteristics in the range of low and moderate voltages are independent of parameter η_0^{decay}. This is in line with the results of the previous analytical analysis [see Eqs. (13) and (14)]. However, at relatively high voltages, distinctions in the *J*–*V* characteristics for different η_0^{decay} is significant although all of them tend to J_0 when *V* approaches to $\hbar\omega_0/e$.

VI. DYNAMIC CONDUCTIVITY

Knowing the *T*–*V* dependences, one can calculate the dynamic conductivity, σ_ω, of a GL under the injection pumping as a function of the signal frequency ω and the applied voltage *V*. To achieve lasing at the frequency ω, the real part of the complex dynamic conductivity at this frequency should be negative: Re $\sigma_\omega < 0$. As shown previously (see, for instance, Refs. 4 and 35), the interband contribution of the nonequilibrium electron-hole plasma with the quasi-Fermi energy μ and the effective temperature *T* is proportional to $\tanh[(\hbar\omega - 2\mu)/4T]$. The intraband contribution to Re σ_ω, which corresponds to the Drude absorption, depends on ω, μ, and *T* as well. It also depends on the time of electron and hole momentum relaxation on impurities and phonons τ. The latter is a function of the energy of electrons and holes ε. The main reason for the $\tau - \varepsilon$ dependence is a linear increase in the density of state in GLs with increasing ε. In this case, $\tau^{-1} = \nu_0(\varepsilon/T_0)$, where ν_0 is the collision frequency of electrons and holes in equilibrium at $T = T_0$. Considering this and taking into account Eq. (1), we can arrive at the following formula[16] approximately valid in the frequency range $\omega \gg \nu_0$:

$$\frac{\mathrm{Re}\sigma_\omega}{\sigma_0} = \tanh\left(\frac{\hbar\omega - eV}{4T}\right) + C\frac{(e^2V^2 + 2\pi^2T^2/3)}{\hbar^2\omega^2}. \quad (22)$$

Here, $\sigma_0 = e^2/4\hbar$ and $C = 2\hbar\nu_0/\pi T_0$. In high quality MGLs (with $\nu_0^{-1} \simeq 20$ ps at $T_0 = 50$ K (Refs. 2 and 3), assuming that $\nu_0 \propto T_0$ (Ref. 36) for $T_0 = 300$ K, one can set $\nu_0 \simeq 3 \times 10^{11}$ s^{-1} and hence, $C \simeq 0.005$. For substantially less perfect GLs with $\nu_0 \simeq 15 \times 10^{11}$ s^{-1}, one obtains $C \simeq 0.025$. These data are used for the calculations of Re σ_ω.

Figure 6 demonstrates the frequency dependences of Re σ_ω/σ_0 calculated using Eq. (22) for different values of parameter η_0^{decay} at different voltages *V* for $\nu_0 \simeq 3 \times 10^{11}$ s^{-1} and $\nu_0 \simeq 15 \times 10^{11}$ s^{-1}. As seen from Fig. 6 at the injection conditions under consideration, the characteristic conductivity

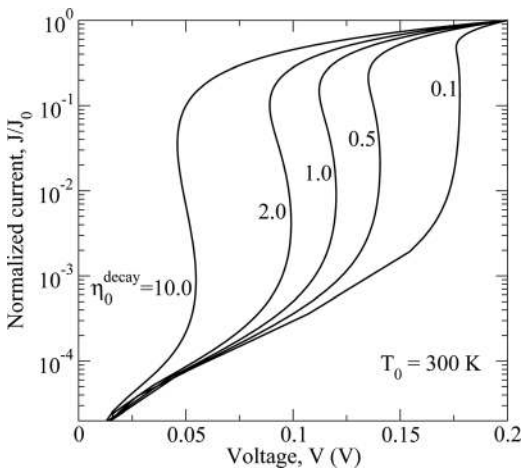

FIG. 5. Normalized current-voltage characteristics for different values of η_0^{decay}.

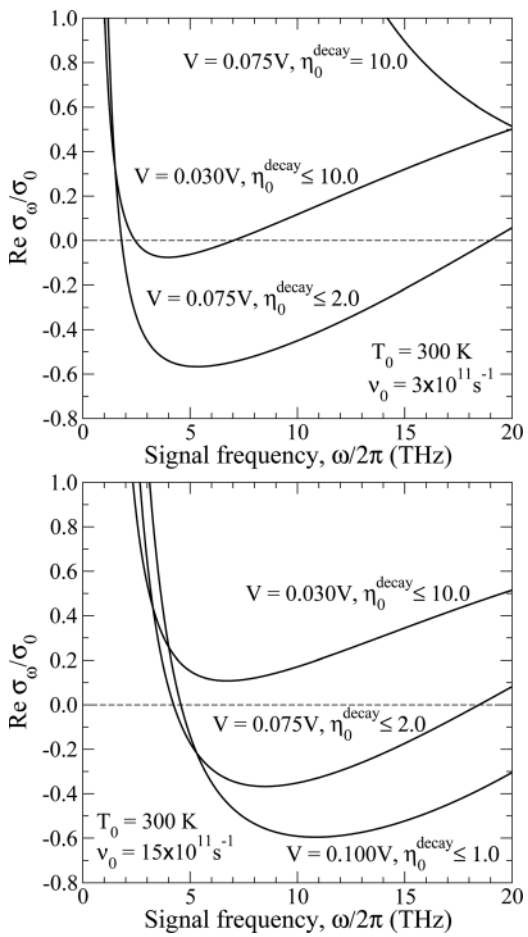

FIG. 6. Dependence of normalized dynamic conductivity Re σ_ω/σ_0 on signal frequency $\omega/2\pi$ for different values of η_0^{decay} and $\nu_0 \simeq 3 \times 10^{11}$ s^{-1} (upper panel) and $\nu_0 \simeq 15 \times 10^{11}$ s^{-1} (lower panel).

σ_0 is much smaller than the dc conductivity in the i-section $\sigma_\omega|_{\omega=0} = \sigma_{00}$. It is also seen that even at relatively large values of parameter η_0^{decay}, the dynamic conductivity can be negative in the THz range of frequencies provided the applied voltage is not so strong to cause the electron-hole plasma and optical phonon system overheating and the ambiguity of the voltage characteristics. This is confirmed by Fig. 7. Figure 7 shows Re σ_ω/σ_0 as a function of the applied voltage. As demonstrated, the range of the signal frequencies where Re $\sigma_\omega < 0$ markedly shrinks and the quatity |Re σ_ω| decreases when either η_0^{decay} or ν_0 increase. In particular, at large values of η_0^{decay}, the achievement of the negative dynamic conductivity and THz lasing can be complicated (at the temperatures $T_0 \sim 300$ K when the optical phonon recombination mechanism dominates). This is because when η_0^{decay} increases, the quantity V_d becomes small. As a result, the optical phonon system is overheated starting from relatively low voltages that leads to an "early" overheating of the electron-hole plasma [see Figs. (3) and (4)]. If the value of Re σ_ω is insufficient to overcome the losses of the THz modes propagating along the GL structure, the structures with MGL can be used. In this case, the net dynamic conductivity of the MGL structure is given by Re $\sigma_\omega \times K$, where K is the number of GLs.[8–10]

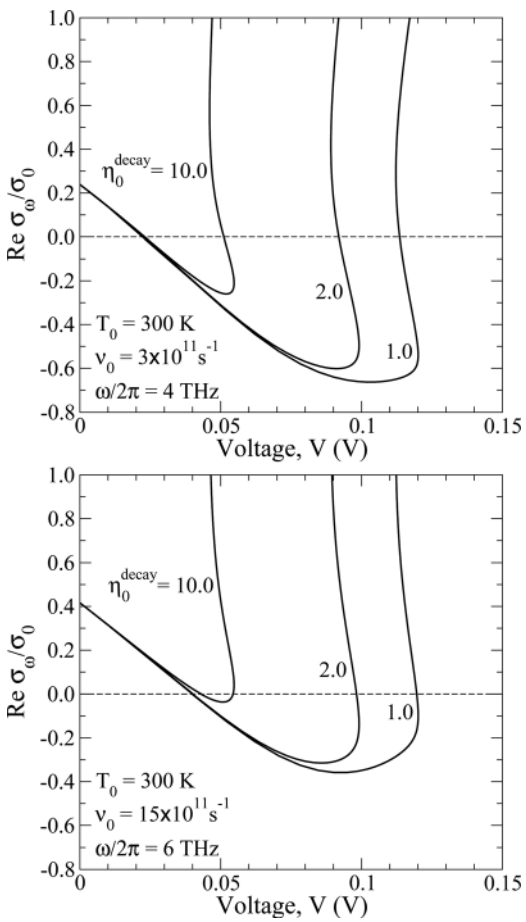

FIG. 7. Normalized dynamic conductivity Re σ_ω/σ_0 vs applied voltage V for different values of η_0^{decay} and $\nu_0 \simeq 3 \times 10^{11}$ s^{-1}, $\omega/2\pi = 4$ THz (upper panel) and $\nu_0 \simeq 15 \times 10^{11}$ s^{-1}, $\omega/2\pi = 6$ THz (lower panel).

VII. LIMITATIONS OF THE MODEL AND DISCUSSION

High density of the electron-hole plasma in the i-section under the injection conditions promotes the quasi-neutrality of this section. The recombination does not significantly affect the uniform distribution of the electron and hole densities in the i-section (assumed above) if the recombination current J is much smaller than the maximum injection current J_m which can be provided by the p- and n-sections. This imposes the condition $J \ll 2J_m$. The latter inequality is equivalent to the condition that the recombination length is longer than the i-section length $2L$. Considering a strong degeneracy of the electron and hole components in the p- and n-sections, respectively, the quantity J_m can be estimated as

$$J_m \simeq \frac{ev_F}{\pi^2\hbar^2}[\mu_i^2 - (\mu_i - eV)^2]. \tag{23}$$

At $T_0 = 300$ K, $2L = 20\,\mu$m, $\mu_i = 0.3$ eV, and $V = 0.1$ V, one obtains $J_0 \simeq 32$ A/cm and $2J_m \simeq 65$ A/cm. As seen from Fig. 5, $J \ll J_0$ at least in the most interesting voltage range, where Re $\sigma_\omega < 0$ (see Fig. 7), the condition $J \ll J_m$ is satisfied.

In the above consideration, we disregarded the leakage current from the i-section to the p- and n-sections. This current includes the tunneling and thermionic components. Both these components depend on the height, μ_i, of the barriers between the p- and i-sections and i- and n-sections and the applied voltage V (see Fig. 2). As shown previously,[37] the tunneling current decreases with increasing width of the p-i- or i-n junction l [see Fig. 2(a)], because it is sensitive to the electric field at the junction.[18] The width in question depends on the geometrical parameters of the structure, in particular on the spatial distributions of donor and acceptors near the junction, and the thickness of the gate layer W_g, as well as the shape of the gates (in the structures with the electrical doping). So, one can assume that this width can be sufficiently large to provide smooth potential distributions at the junctions. The effective height of the barriers at the p-i- and i-n-junctions, which determines the thermionic electron and hole current over these barriers, is equal to $\Delta = \mu_i - 2\mu = \mu_i - eV$. It can be small at elevated values of the quasi-Fermi energy μ which are necessary to achieve the negative dynamic conductivity (see, for instance, Refs. 4, 6, 9, and 10), i.e., in the most interesting case. This, in turn, implies that the electric field at the junctions and, hence, the tunneling current is decreased. In this case, the thermionic leakage current dominates over the tunneling leakage current and the latter is disregarded in the following estimates.

Taking into account, the height of the barrier Δ, for the contribution of thermionic current through the junctions to the net terminal current, one can obtain

$$J_{th} = \frac{4ev_F}{\pi^2}\left(\frac{T^2}{\hbar^2 v_F^2}\right)^2\left[\exp\left(\frac{eV-\mu_i}{T}\right) - 1\right]$$
$$= 2ev_{th}\Sigma_0\left(\frac{T}{T_0}\right)^2\left[\exp\left(\frac{eV-\mu_i}{T}\right) - 1\right]. \tag{24}$$

Here, $v_{th} = (12/\pi^3)v_F$. Comparing J and J_{th} given by Eqs. (5) and (24), respectively, one can conclude that the leakage

(thermionic) current is small in comparison with the current associated with the optical phonon recombination if $(v_{th}\tau_0/L)\exp(-\mu_i/T) \ll \exp(-\hbar\omega_0/T)$ or

$$\mu_i - \hbar\omega_0 > T \ln\left[\left(\frac{v_{th}\tau_0}{L}\right)\left(\frac{T}{T_0}\right)^2\right]. \quad (25)$$

Assuming that $\tau_0 \sim 10^{-12}$ s, factor $(v_{th}\tau_0/L)$ in Eq. (21) is small when the length of the i-section $2L \gtrsim 1\mu$m, i.e., at fairly practical values of $2L$. Therefore, neglect of the thermionic leakage in our calculations in the above sections is justified when $\mu_i > \hbar\omega_0 \simeq 0.2$ eV (more precisely, when $\mu_i - \hbar\omega_0 > T$). At $T \gtrsim T_0$, the latter inequality means that the donor and acceptor density in the pertinent sections should be

$$\Sigma_i > \frac{1}{\pi}\left(\frac{\omega_0}{v_F}\right)^2 \simeq 3.3 \times 10^{12}\ \text{cm}^{-2}. \quad (26)$$

In the case of the devices with the electrically induced p- and n-section, the analogous condition sounds as

$$V_g > \frac{4eW_g}{æ}\left(\frac{\omega_0}{v_F}\right)^2. \quad (27)$$

Setting $æ = 4$ and $W_g = 10$ nm, the latter condition corresponds to $V_g > 1.5$ V.

At a strong heating of the electron-hole plasma, say, at $V = \hbar\omega_0/e$, using Eq. (15), condition (25) is replaced by

$$\mu_i > \hbar\omega_0 \frac{\ln(v_{th}\tau_0/L)}{\ln\left(\dfrac{1+\eta_0^{decay}+\mathcal{N}_0^{eq}}{\eta_0^{decay}+\mathcal{N}_0^{eq}}\right)}. \quad (28)$$

The latter inequality can impose somewhat stricter limitation on the values of μ_i and Σ_i than those given by Eqs. (25) and (26) if $\eta_0^{decay} > 1$.

It is notable that an effective confinement of the injected electrons and holes in the i-section by the barriers at p-i- and i-n-junctions in the GL structures under consideration can be realized by relatively low doping levels in p- and n-sections in comparison with structures with two-dimensional (2D) electron plasma in quantum wells on the base of the standard semiconductors. Indeed, the barrier height at $V = 0$ in the doped section of GL is equal to $\Delta = \mu_i - eV$. In standard 2D systems with the electron effective mass m^* and the energy gap Δ_g, the barrier height is equal to $\Delta^* = \Delta_g + \mu_i^* - eV^*$, where $\mu_i^* \simeq \pi\hbar^2\Sigma_i^*/m^*$. To achieve the same value of the quasi-Fermi energy μ in the standard 2D system as in GLs, one needs to apply the voltage $V^* = V + \Delta_g/e$. To provide, for example, the values $\mu_i = \mu_i^* = 0.3$ eV, one needs $\Sigma_i \simeq 7.33 \times 10^{12}$ cm^{-2} and $\Sigma_i^* \simeq 3.82 \times 10^{13}$ cm^{-2}, respectively. Thus, in the standard 2D electron systems, the doping should be five times higher (for $m = 4 \times 10^{-29}$ g). This is due to lower density of states in massless GLs near the Dirac point compared to that in the standard 2D structures with $m \neq 0$. Since the effective mass of holes M^* in the standard semiconductors is markedly larger than m^*, the realization of the barrier height at the p-i-junction sufficient for the effective confinement of electrons at elevated temperatures requires fairly heavy doping. Thus, in contrast to the standard 2D structures, the thermionic leakage current in the GL or MGL p-i-n structures under consideration can be sufficiently small without the employment of wide-gap p- and n-sections. In passing, it should be mentioned that an extra confinement of the injected electrons and holes can be achieved if the p- and n-sections constitute arrays of graphene nanowires (doped or with electrically induced high electron and hole densities), so that the p-i-n structures considered above are replaced by the P-i-N structures.

One needs to stress that the assumptions (used in the above model) that the electron-hole plasma in the active region is virtually uniform as well as that the recombination current exceeds the leakage current are rather common in simplified models (the so-called rate-equation models) of in standard injection laser structures with the double injection (see, for instance, Refs. 38 and 39).

As follows from the above calculations, the effective electron-hole and optical phonon temperature can be very high at $V \sim \hbar\omega_0/e$ and be accompanied by effects associated with the *S*-shape characteristics. In this case, an expression for the rate of optical phonon decay $(\mathcal{N}_0 - \mathcal{N}_0^{eq})/\tau_0^{decay}$ used in Eq. (7) might be oversimplified due to a strong anharmonic lattice vibration. Possibly, the effects related to a strong anharmonism can be taken into account by a proper choice (renormalization) of parameters τ_0^{decay} and η_0^{decay}. In the above treatment, for simplicity, only one type of optical phonons with $\hbar\omega_0 \simeq 0.2$ eV was taken in to account. However, due to closeness of the optical phonon frequencies of different type in GLs and MGLs, the pertinent generalization of the model, adding computational complexity, should not lead to a marked change in the obtained results. Apart from this, at large effective temperatures, the radiative recombination and cooling (due to the radiative transfer of the energy outside the structure) can become essential,[40–42] resulting in a limitation of these temperatures and affecting the *S*-shape dependences. This means that considering the range or relatively high applied voltages and, hence, strong injection, our purely "optical phonon" model should be generalized. However, this concerns not particularly interesting situations in which the dynamic conductivity is not negative.

As demonstrated, the main potential obstacles in the realization of negative dynamic conductivity and THz lasing in the injection GL and MGL structures at the room (or slightly lower) temperatures might be the intraband photon (Drude) absorption and the optical phonon heating. These effects are characterized by parameters $C \propto \nu_0$ and $\eta_0^{decay} \propto \tau_0^{decay}$, respectively. As for parameter C, it can be sufficiently small in perfect MGL structures like those studied in Ref. 2, so the problem of intraband absorption can be overcome. However, if real values of parameter η_0^{decay} cannot be decreased to an appropriate level $\left(\eta_0^{decay} \lesssim 1\right)$, the achievement of room temperature THz lasing in the structures under consideration might meet problems. In the case of such a scenario, the utilization of lower temperatures, at which the recombination and energy relaxation is associated with different mechanisms, can become indispensable.

VIII. CONCLUSIONS

In conclusion, we have studied theoretically the effect of population inversion associated with the electron and hole injection in GL and MGL p-i-n structures at the room and slightly lower temperatures when the interaction with optical phonons is the main mechanism of the recombination and energy relaxation. In the framework of the developed model, the electron-hole and optical phonon effective temperatures and the current-voltage characteristics have been calculated as functions of the applied voltage and the structure parameters. It has been demonstrated that the injection can lead to cooling of the injected electron-hole plasma in the device i-section to the temperatures lower than the lattice temperature at low and moderate voltages, whereas the voltage dependences can be ambiguous exhibiting the S-shape behavior at elevated voltages. The variations of the electron-hole effective temperature with increasing applied voltage are accompanied with an increase in the optical phonon effective temperature. Using the obtained voltage dependences, we have calculated the dynamic conductivity and estimated the ranges parameters and signal THz frequencies where this conductivity is negative. The electron-hole cooling might substantially promote the realization of THz lasing at elevated ambient temperatures. In summary, we believe that the obtained results instill confidence in the future of graphene-based injection THz lasers although their realization might require a thorough optimization.

ACKNOWLEDGMENTS

The authors are grateful to A. Satou for numerous useful discussions. This work was supported by the Japan Science and Technology Agency, CREST and by the Japan Society for Promotion of Science, Japan.

[1]A. H. C. Neto, F. Guinea, N. M. R. Peres, K. S. Novoselov, and A. K. Geim, Rev. Mod. Phys. **81**, 109 (2009).
[2]M. Sprinkle, D. Suegel, Y. Hu, J. Hicks, A. Tejeda, A. Taleb-Ibrahimi, P. Le Fevre, F. Bertran, S. Vizzini, H. Enriquez, S. Chiang, P. Soukiassian, C. Berger, W. A. de Heer, A. Lanzara, and E. H. Conrad, Phys. Rev. Lett. **103**, 226803 (2009).
[3]M. Orlita and M. Potemski, Semicond. Sci. Technol. **25**, 063001 (2010).
[4]V. Ryzhii, M. Ryzhii, and T. Otsuji, J. Appl. Phys. **101**, 083114 (2007).
[5]F. Rana, IEEE Trans. Nanotechnol. **7**, 91 (2008).
[6]A. Dubinov, V. Ya. Aleskin, M. Ryzhii, and V. Ryzhii, Appl. Phys. Express **2**, 092301 (2009).
[7]B. Dora, E. V. Castro, and R. Moessner, Phys. Rev. B **82**, 125441 (2010).
[8]A. A. Dubinov, V. Ya. Aleshkin, V. Mitin, T. Otsuji, and V. Ryzhii, J. Phys.: Condens. Matter **23**, 145302 (2011).
[9]V. Ryzhii, M. Ryzhii, A. Satou, T. Otsuji, A. A. Dubinov, and V. Ya. Aleshkin, J. Appl. Phys. **106**, 084507 (2009).
[10]V. Ryzhii, A. A. Dubinov, T. Otsuji, V. Mitin, and M. S. Shur, J. Appl. Phys. **107**, 054505 (2010).
[11]M. Ryzhii and V. Ryzhii, Jpn. J. Appl. Phys. **46**, L151 (2007).
[12]A. Satou, F. T. Vasko, and V. Ryzhii, Phys. Rev. B **78**, 115431 (2008).
[13]A. Satou, T. Otsuji, and V. Ryzhii, Jpn. J. Appl. Phys. **50**, 070116 (2011).
[14]T. Otsuji, S. A. Boubanga-Tombet, S. Chan, A. Satou, and V. Ryzhii, Proc. SPIE **8023**, 802304 (2011).
[15]S. Boubanga-Tombet, S. Chan, A. Satou, T. Otsuji, and V. Ryzhii, e-print arXiv:1011.2618.
[16]V. Ryzhii, M. Ryzhii, V. Mitin, A. Satou, and T. Otsuji, Jpn. J. Appl. Phys. **50**(9), 094001 (2011).
[17]R. Kim, V. Perebeinos, and P. Avouris, Phys. Rev. B **84**, 075449 (2011).
[18]V. V. Cheianov and V. I. Fal'ko, Phys. Rev. B **74**, 041403(R) (2006).
[19]M. Ryzhii, V. Ryzhii, T. Otsuji, V. Mitin, and M. S. Shur, Phys. Rev. B **82**, 075419 (2010).
[20]F. Rana, P. A. George, J. H. Strait, S. Shivaraman, M. Chanrashekhar, and M. G. Spencer, Phys. Rev. B **79**, 115447 (2009).
[21]A. Satou, F. T. Vasko, and V. Ryzhii, Phys. Rev. B **78**, 115431 (2008).
[22]M. S. Foster and I. L. Aleiner, Phys. Rev. B **79**, 085415 (2009).
[23]D. M. Basko, S. Piscanec, and A. C. Ferrari, Phys. Rev. B **80**, 165413 (2009).
[24]F. T. Vasko and V. V. Mitin, e-print arXiv:1107.2708.
[25]V. Ryzhii, M. Ryzhii, and T. Otsuji, e-print arXiv:1108.2077.
[26]J. Martin, N. Akerman, G. Ulbricht, T. Lohmann, J. H. Smet, K. von Klitzing, and A. Yacoby, Nature Phys. **4**, 144 (2008).
[27]Y. Zhang, V. W. Brar, C. Girit, A. Zett, and M. F. Cromme, Nature Phys. **5**, 722 (2009).
[28]J. M. Poumirol, W. Escoffer, A. Kumar, M. Goiran, R. Raquet, and J. M. Broto, New. J. Phys. **12**, 083006 (2010).
[29]P. Parovi-Azar, N. Nafari, and M. R. R. Tabat, Phys. Rev. B **83**, 165434 (2011).
[30]H. Wang, J. H. Strait, P. A. George, S. Shivaraman, V. D. Shields, M. Chandrashekhar, J. Hwang, F. Rana, M. G. Spencer, C. S. Ruiz-Vargas, and J. Park, Appl. Phys. Lett. **96**, 081917 (2010).
[31]C. Auer, F. Schurer, and C. Ertler, Phys. Rev. B **74**, 165409 (2006).
[32]G. Pennington, S. J. Kilpatrick, and A. E. Wickenden, Appl. Phys. Lett. **93**, 093110 (2008).
[33]M. Steiner, M. Freitag, V. Perebeinos, J. C. Tsang, J. P. Small, M. Kinoshita, D. Yuan, J. Liu, and P. Avouris, Nat. Nanotechnol. **4**, 320 (2009).
[34]P. A. George, J. Strait, J. Dawlaty, S. Shivaraman, M. Chandrashekhar, F. Rana, and M. G. Spencer, Nano Lett. **8**, 4248 (2008).
[35]L. A. Falkovsky and A. A. Varlamov, Eur. Phys. J. B **56**, 281 (2007).
[36]L. A. Falkovsky, Phys. Rev. B **75**, 03349 (2007).
[37]V. Ryzhii, M. Ryzhii, and T. Otsuji, Phys. Status Solidi A **205**, 1527 (2008).
[38]G. P. Agrawal and N. K. Dutta, *Semiconductor Lasers* (Van Nostrand Reinhold, New York, 1993).
[39]L. A. Coldren and S. W. Corzine, *Diode Lasers and Photonic Integrated Circuits* (Wiley, New York, 1995).
[40]F. T. Vasko and V. Ryzhii, Phys. Rev. B **77**, 195433 (2008).
[41]P. N. Romanets, F. T. Vasko, and M. V. Strikha, Phys. Rev. B **79**, 033406 (2009).
[42]O. G. Balev, F. T. Vasko, and V. Ryzhii, Phys. Rev. B **79**, 165432 (2009).